Theta and Gamma Coherence Along the Septotemporal Axis of the Hippocampus

Helen R. Sabolek, Stephanie C. Penley, James R. Hinman, Jamie G. Bunce, Etan J. Markus, Monty Escabi and James J. Chrobak

J Neurophysiol 101:1192-1200, 2009. First published 31 December 2008; doi:10.1152/jn.90846.2008

You might find this additional info useful...

This article cites 56 articles, 14 of which can be accessed free at:
http://jn.physiology.org/content/101/3/1192.full.html#ref-list-1

This article has been cited by 1 other HighWire hosted articles
Septotemporal variation in dynamics of theta: speed and habituation
James R. Hinman, Stephanie C. Penley, Lauren L. Long, Monty A. Escabí and James J. Chrobak
J Neurophysiol, June , 2011; 105 (6): 2675-2686.
[Abstract] [Full Text] [PDF]

Updated information and services including high resolution figures, can be found at:
http://jn.physiology.org/content/101/3/1192.full.html

Additional material and information about ***Journal of Neurophysiology*** can be found at:
http://www.the-aps.org/publications/jn

This infomation is current as of September 19, 2011.

Journal of Neurophysiology publishes original articles on the function of the nervous system. It is published 12 times a year (monthly) by the American Physiological Society, 9650 Rockville Pike, Bethesda MD 20814-3991. Copyright © 2009 by the American Physiological Society. ISSN: 0022-3077, ESSN: 1522-1598. Visit our website at http://www.the-aps.org/.

Downloaded from jn.physiology.org on September 19, 2011

J Neurophysiol 101: 1192–1200, 2009.
First published December 31, 2008; doi:10.1152/jn.90846.2008.

Theta and Gamma Coherence Along the Septotemporal Axis of the Hippocampus

Helen R. Sabolek,[1] Stephanie C. Penley,[1] James R. Hinman,[1] Jamie G. Bunce,[1] Etan J. Markus,[1] Monty Escabi,[2] and James J. Chrobak[1]

[1]*Departments of Psychology and* [2]*Biomedical Engineering, University of Connecticut, Storrs, Connecticut*

Submitted 1 August 2008; accepted in final form 28 December 2008

Sabolek HR, Penley SC, Hinman JR, Bunce JG, Markus EJ, Escabi M, Chrobak JJ. Theta and gamma coherence along the septotemporal axis of the hippocampus. *J Neurophysiol* 101: 1192–1200, 2009. First published December 31, 2008; doi:10.1152/jn.90846.2008. Theta and gamma rhythms synchronize neurons within and across brain structures. Both rhythms are widespread within the hippocampus during exploratory behavior and rapid-eye-movement (REM) sleep. How synchronous are these rhythms throughout the hippocampus? The present study examined theta and gamma coherence along the septotemporal (long) axis of the hippocampus in rats during REM sleep, a behavioral state during which theta signals are unaffected by external sensory input or ongoing behavior. Unilateral entorhinal cortical inputs are thought to play a prominent role in the current generation of theta, whereas current generation of gamma is primarily due to local GABAergic neurons. The septal 50% (4–5 mm) of the dentate gyrus (DG) receives a highly divergent, unilateral projection from any focal point along a lateral band of entorhinal neurons near the rhinal sulcus. We hypothesized that theta coherence in the target zone (septal DG) of this divergent entorhinal input would not vary, while gamma coherence would significantly decline with distance in this zone. However, both theta and gamma coherence decreased significantly along the long axis in the septal 50% of the hippocampus across both DG and CA1 electrode sites. In contrast, theta coherence between homotypic (e.g., DG to DG) sites in the contralateral hemisphere (~3–5 mm distant) were quite high (~0.7–0.9), much greater than theta coherence between homotypic sites 3–5 mm distant (~0.4–0.6) along the long axis. These findings define anatomic variation in both rhythms along the longitudinal axis of the hippocampus, indicate the bilateral CA3/mossy cell projections are the major determinant of theta coherence during REM, and demonstrate that theta coherence varies as a function of anatomical connectivity rather than physical distance. We suggest CA3 and entorhinal inputs interact dynamically to generate theta field potentials and advance the utility of theta and gamma coherence as indicators of hippocampal dynamics.

INTRODUCTION

Theta (6–12 Hz) and gamma (40–110 Hz) oscillations are rhythmic fluctuations in field potentials and neuronal discharge that are posited to serve computational and cognitive functions (Gray 1994; Hasselmo 2005; Kahana et al. 2001; Lisman 2005). Both rhythms are evident in a number of brain structures and are quite prominent within the rodent hippocampus (Bland 1986; Csicsvari et al. 2003; Hyman et al. 2005; Leung 1984; Petsche et al. 1962; Vertes and Kocsis 1997). Theta and gamma can be reproduced with some fidelity in brain slices, allowing for the study of cellular and local circuit mechanisms (Cunningham et al. 2003; Dickson et al. 2000; Glovelli et al. 2005) and how rhythmic activity contributes to synaptic plasticity (e.g., Lin et al. 2005). In contrast, the spatial organization and degree of synchrony in vivo have been less well studied.

Within the rodent hippocampus, it is generally assumed that theta is coherent across regions (e.g., CA1, dentate gyrus) and along the septotemporal (long) axis. Thus theta signals from a single electrode site are typically used as a temporal reference for related neural activity throughout the entire brain (Chrobak and Buzsaki 1998; Hyman et al. 2005; Jones and Wilson 2005; Maurer et al. 2005). However, there is significant variation in the amplitude and coherence across lamina (Bragin et al. 1995; Buzsaki et al. 1983, 1986; Kocsis et al. 1999; Leung 1984). The degree of variation in coherence along the long axis has not been well studied (see, however, Bragin et al. 1995; Bullock et al. 1990).

Unilateral entorhinal cortical inputs are thought to play the most prominent role in the current generation of theta, while the contribution of bilateral CA3 associational and commissural inputs is thought to be relatively small (Brankack et al. 1993; Buzsaki 2002; Buzsaki et al. 1983, 1986). Other studies have shown considerable coherence across hemispheres (Buzsaki et al. 2003; Koscis et al. 1994), suggesting a larger role for currents generated by the bilateral CA3 and hilar mossy cell (commissural) inputs. Entorhinal afferents define three areal zones along the septotemporal axis of the dentate gyrus (DG) (Dolorfo and Amaral 1998a,b) with the septal 50% receiving input from a lateral band of entorhinal neurons near the rhinal sulcus (Dolorfo and Amaral 1998a) (see also Fig. 1*C*). Based on the facts the entorhinal afferents provide a prominent input for hippocampal theta and that the septal 50% of the HPC receives a highly divergent input from the lateral band of the entorhinal cortex, we asked whether theta and gamma coherence varied significantly within the target zone of this projection (septal 50% of the DG) during rapid-eye-movement (REM) sleep. We choose REM sleep as a baseline condition where theta signals would not be influenced by changes in ongoing behavior and when external sensory stimuli would have a minimal influence.

We implanted electrode arrays along the septotemporal axis and in the contralateral hemisphere and subsequently recorded hippocampal theta signals during multiple REM sleep sessions. We observed a larger than expected decrease in theta coherence along the septotemporal axis than one might expect based on the fact that this portion of the DG receives projections from the same band of the entorhinal cortex. Further, theta coher-

Address for reprint requests and other correspondence: J. J. Chrobak, Dept. of Psychology, University of Connecticut, Storrs, CT 06269 (E-mail: james.chrobak@uconn.edu).

The costs of publication of this article were defrayed in part by the payment of page charges. The article must therefore be hereby marked "*advertisement*" in accordance with 18 U.S.C. Section 1734 solely to indicate this fact.

0022-3077/09 $8.00 Copyright © 2009 The American Physiological Society

Downloaded from jn.physiology.org on September 19, 2011

ence was considerably higher (~0.7–0.9) between homotypic (e.g., DG-DG) locations across hemispheres than between equally or less distant longitudinal sites in the same hemisphere. The latter demonstrates that theta varies as a function of anatomical connectivity rather than physical distance and suggests a prominent influence of the bilateral projections from CA3 and mossy cells in theta current generation and theta coherence during REM sleep. These findings are discussed with respect to the neuroanatomical circuits generating theta and gamma rhythms, functional differentiation along the septotemporal (long) axis, and how understanding the variability in theta and gamma signals across brain sites may offer insight into the role of rhythmic activity in cognition (e.g., Raghavachari et al. 2005).

METHODS

Animals and surgeries

Twenty adult male rats (12 Sprague-Dawley and 8 Fisher-344) were used in this study. The animals were housed on a 12-h/12-h light-dark cycle, in a temperature-controlled room. All procedures were performed in accordance with the guidelines set forth by University of Connecticut's Institutional Animal Care and Use Committee and National Institutes of Health.

Rats were anesthetized with a ketamine cocktail (4 ml/kg) consisting of (in mg/ml): 25 ketamine, 1.3 xylazine, and 0.25 acepromazine. After a midline scalp incision, two to four burr holes were drilled in the skull over the hippocampal formation and four electrode arrays of four linearly spaced 50 um tungsten wires (16 total electrodes; California Fine Wire, Grover Beach, CA), arranged and spaced using fused silica tubing (Polymicro Tubing, Phoenix, AZ), were positioned into the hippocampus along the septotemporal extent of the hippocampus. Three arrays were positioned into one hippocampus at distinct septotemporal positions and a fourth array was positioned in the contralateral septal hippocampus. The targeted positions were (relative to bregma) : AP: −2.5, −5.0, −7.5 mm; ML: 1.5, 2.5, 4.0; DV, 3–7.00 mm.

The majority of electrodes were located below the hippocampal fissure in the molecular layer, the granule cell layer and the hilus of the DG (see Fig. 1). In some experiments, electrodes were targeted toward the superficial aspect of CA1. All electrodes were attached to female pins (Omnetics, Minneapolis, MN) secured in a rectangular five by four pin array. Two stainless steel watch screws driven into the skull above the cerebellum served as indifferent and ground electrodes. Two or more additional support screws were positioned over the anterior aspect of the skull and the entire ensemble was secured with dental acrylic.

Electrophysiological recordings and data analysis

Following implantation of electrodes, rats were allowed ≥1 wk to recover. Recordings were obtained from rats during naturally occurring REM episodes during the light phase of their daily sleep cycle. Thirty seconds of data, composed of 10 nonoverlapping portions (3 s each) of artifact free theta activity with a peak frequency between 6 and 8 Hz, were selected from each REM episode. REM episodes ranged from 30–120 s in duration but only one 30-s concatenated epoch was used from each REM episode. We used an instantaneous FFT to ensure that each selected epoch of activity, the peak frequency remained in the 6- to 8-Hz range throughout, corresponding with tonic REM. Individual 3-s segments from each channel were concatenated into a single continuous string of data. To do this, a cross fading procedure was applied where the first and last 100 ms of each 3-s data segment was ramped or faded respectively with a smooth B-spline window with continuous second-order derivatives (Roark and Escabi 1999). Adjacent start and end blocks from subsequent segments were then overlapped and morphed by adding the signals overlapping the ramp and fade regions. Power spectral density estimates were then obtained in Matlab using Welch's averaged modified periodogram method (Welch 1967).

Coherence values (Bullock et al. 1990) for each channel pair were computed using the Welch periodogram estimation procedure with a spectral resolution of ~2 Hz. Coherence is a measure of the linear association between two signals as a function of frequency. Two signals can differ in amplitude and phase and still be highly coherent assuming the *relative* amplitude and phase *between* the two signals remains constant, and coherence is not influenced by obvious differences in the waveform of the signal. Note that waveform shapes prototypically vary across different laminar positions. Waveforms recorded in CA1 are characteristically sine-like, while triangular waveforms are more characteristic of DG (see Fig. 1*E*). It should be noted that due to characteristics of Fourier transform, triangular waves at theta frequency can induce harmonics at that artificially increase power and coherence in the beta band (16–24 Hz). However, over a wide theta range (2–14 Hz), we have found no coherence differences between artificially generated sine-waves and triangular waves.

Coherence, $C_{xy}(\omega)$, between two signals, x and y, is equivalent to the square root of the squared cross-spectrum $[P_{xy}(\omega)]$ magnitude normalized by the averaged power spectrum of the individual signals $[P_{xx}(\omega)$ and $P_{yy}(\omega)]$

$$C_{xy}(\omega) = \sqrt{\frac{|P_{xy}(\omega)|^2}{P_{xx}(\omega) \cdot P_{yy}(\omega)}}$$

To ensure that the measured coherence values were not due to chance alone, a significance estimation procedure was devised in which the coherence estimate was compared with that of signals with identical magnitude spectrum but with zero phase coherence. For each channel pair, the cumulative distribution of the frequency-dependent coherence values was created by circularly phase shifting one signal in the pair by a random amount, calculating the coherence for the shifted signals, and bootstrapping the procedure 250 times (Efron and Tibshirani 1993). This procedure guarantees that the signal spectrums are identical but have no linear association because the phase or time information has been removed. The coherence distribution was used to determine a threshold for each frequency band (2-Hz resolution) below which 95% of the shifted null hypothesis coherence values fell. Thus only regions of the nonshuffled signal coherences falling above the 95% threshold were considered significant. For each channel pair, the statistically significant area in the theta (6–10 Hz), gamma (40–110 Hz), beta (16–30 Hz), and gamma sub-bands (31–50, 51–70, 71–90, and 91–110 Hz) were calculated (Fig. 1*D*), and normalized by the frequency range (expressed as average coherence value per Hz) to facilitate comparison of different frequency ranges

$$C_{\text{Ave}} = \frac{1}{\omega_2 - \omega_1} \int_{\omega_1}^{\omega_2} C_{xy}(\omega) \mathrm{d}\omega$$

where ω_1 and ω_2 correspond to the lower and upper frequency range for each band. Average coherence values were normalized relative to the maximum possible significant coherence for each frequency range, which consisted of the total area above the 95% threshold within a given frequency range. The resulting normalized coherence values fall between 0 and 1.0. Normalized coherence values for each channel pair were then analyzed as a function of laminar position of electrodes and the distance between each electrode pair, using univariate ANOVAs followed by Tukey HSD tests or paired *t*-test.

Histology

Following the completion of recording, rats were anesthetized with Euthasol (sodium pentobarbital solution) and transcardially perfused

Downloaded from jn.physiology.org on September 19, 2011

with ice-cold saline followed by 4% paraformaldehyde in 0.1 M phosphate buffer (pH 7.2). Brains were sliced (50-μm sections) using a vibratome (Vibratome Series 1500), mounted, and Nissl stained using thionin. All electrode positions were verified and categorized according to laminar and septotemporal position. Septotemporal distances between electrode positions were determined by noting the location of each electrode position on a flatmap representation of the hippocampus (Swanson 1978). Each section of a flatmap represents ~200 μm of tissue, and so fairly accurate approximations of the relative distance between electrodes could be determined by counting the number of sections between two electrodes. Photomicrographs of relevant electrode tracks were captured using a Nikon microscope connected to a Spot RT camera system, digitized, and prepared for presentation using Adobe Photoshop 7.0.

RESULTS

We targeted our electrodes to the DG, which included positions in the dendritic field of the granule cells (molecular layer), the granule cell layer and within the hilus ($n = 93$ sites; see Fig. 1). Additional sites ($n = 24$) located in the superficial aspect of CA1 were recorded in some animals. Theta oscillations (0.2–1.0 mV) were present in all sites sampled during REM sleep and power spectral analyses evidenced clear theta peaks (Fig. 1, *B, D*, and *E*). Broadband (40–110 Hz) gamma oscillations were most prominent in the DG and particularly pronounced in the hilar region (0.1–0.4 mV). Dentate and hilar sites nearest to the apex (proximal) of the DG evidenced large gamma waves as well as clear theta waves, while hilar sites located further from the apex (distal), near the polymorphic cells of the hilus and the CA3c border, exhibited less robust theta waves (see Fig. 1*E*) and often exhibited larger amplitude gamma. Theta was much less coherent within hilar (HIL) sites (see Fig. 2, *A* and *B*), and thus we analyzed data from these sites separately from other DG sites (Hil $n = 26$, DG $n = 67$). Gamma coherence was notably reduced between DG sites and hilar sites (Fig. 2, *A* and *C*), further illustrating the variability in theta/gamma signals across the laminar (DG vs. HIL) and proximodistal axis (position relative to apex) of the dentate. Smaller and more variable amplitude gamma oscillations (<0.15 mV) could also be observed near the CA1 pyramidal cell layer (see Fig. 1*E* for laminar variation in theta signals). Note that obvious differences in wave shape do not influence coherence measurement. Thus the more sine wave shape of CA1 signals and triangular shape of DG signals do not effect the coherence measurement over a wide range of frequencies (see METHODS for additional comments).

Theta coherence

LAMINAR POSITION. We observed average theta coherence values of 0.71 ± 0.02 ($n = 131$) between all electrode pairs within 1 mm distance (Fig. 2*A*). Coherence varied according to laminar position and was higher for electrode pairs in similar laminar positions [DG to DG (0.88 ± 0.02; $n = 49$) and CA1 to CA1 (0.89 ± 0.04; $n = 5$)] than between sites in the DG and CA1 (0.78 ± 0.03; $n = 27$). Theta within hilar pairs was less coherent (0.64 ± 0.09, $n = 11$). As noted in the preceding text, theta coherence between hilar and DG pairs was significantly lower (0.38 ± 0.04, $n = 20$) than between DG and CA1 pairs (0.78 ± 0.03, $P < 0.001$; see Fig. 2*A*). Except for the degree of variability of theta and gamma coherence across hilar to dentate sites, these data are consistent with the profile reported by Kocsis and colleagues (1999).

SEPTOTEMPORAL (LONG AXIS) POSITION. Given that the exact septotemporal position of electrode arrays varied from animal to animal, we present the long axis data in two ways: first, as a function of physical distance within a hemisphere regardless of septotemporal position (Fig. 2), and second, grouped into categories within the septal 25th, 50th, and 75th percentiles of the long axis (Fig. 3). Because there can be no "reference" recording electrode across animals, data are compared across physical distance irrespective of septotemporal position (Fig. 2) or in comparison to the septal 25% of the hippocampus, the later serving as a reference region (Fig. 3). Theta coherence gradually decreased with distance across DG-DG electrode pairs (see Fig. 2*B*). When we divided distance into one mm categories (e.g., <1, 1–2, 2–3 mm, etc.), we observed a significant effect of distance with significant decreases observed at distances >3 mm [$F(4,80) = 15.36$, $P < 0.001$; Fig. 2*B*]. At distances of ≥3 mm, theta coherence between DG-DG pairs decreased to 0.44 ± 0.07 as compared with 0.88 ± 0.02 within 1 mm. A similar decrease was seen between CA1–CA1 pairs [$F(3,7) = 5.31$, $P < 0.05$]. Thus at distances of ≥3 mm, coherence along CA1 pairs decreased to 0.70 ±0.11 (see Fig. 3*C*) as compared with 0.89 ± 0.05 at distances <1 mm.

Figure 3 illustrates coherence along the septotemporal axis by dividing the DG into quartiles. We had assumed that theta coherence would be consistent across the septal 50% of the DG based on the topography of entorhinal input. Examining the data for DG sites alone, there was a significant drop in coherence between the most septal quartile and second quartile, as well as between the first and third quartiles [$F(2,71) = 29.64$, $P < 0.001$]. Thus even within the target zone of the lateral entorhinal band input, which innervates the first and second quartiles, there was a significant decrease in theta coherence.

Interhemispheric coherence

The significant decrease in theta coherence as a function of distance within one hemisphere contrasts with the high coherence present between homotypic sites in the contralateral hemisphere (at similar longitudinal and laminar positions). Coherence in homotypic sites across hemispheres [DG (0.81 ± 0.02; $n = 55$), CA1 (0.91 ± 0.02; $n = 12$), and hilus (0.47 ± 0.07, $n = 6$)] was similar to coherence 1–2 mm away in the same hemisphere (compare Fig. 2*A* with Fig. 3*B*). Further, theta coherence across hemispheres (4–6 mm physical distance) was significantly higher than coherence at distances >3 mm within the same hemisphere for the CA1 and DG ($P < 0.001$), but not the hilar region ($P = 0.37$), Fig. 3*C*). It should be noted that we only positioned one array in the contralateral hemisphere and only in the septal hippocampus. Thus these data demonstrate only the high level of coherence across hemispheres in the septal hippocampus.

Gamma coherence

Gamma is typically defined in a broad band across ~40–110 Hz with the dominant frequency varying considerably. Gamma coherence, as expected, decreased more rapidly than theta coherence along the septotemporal axis. As illustrated in Fig.

Downloaded from jn.physiology.org on September 19, 2011

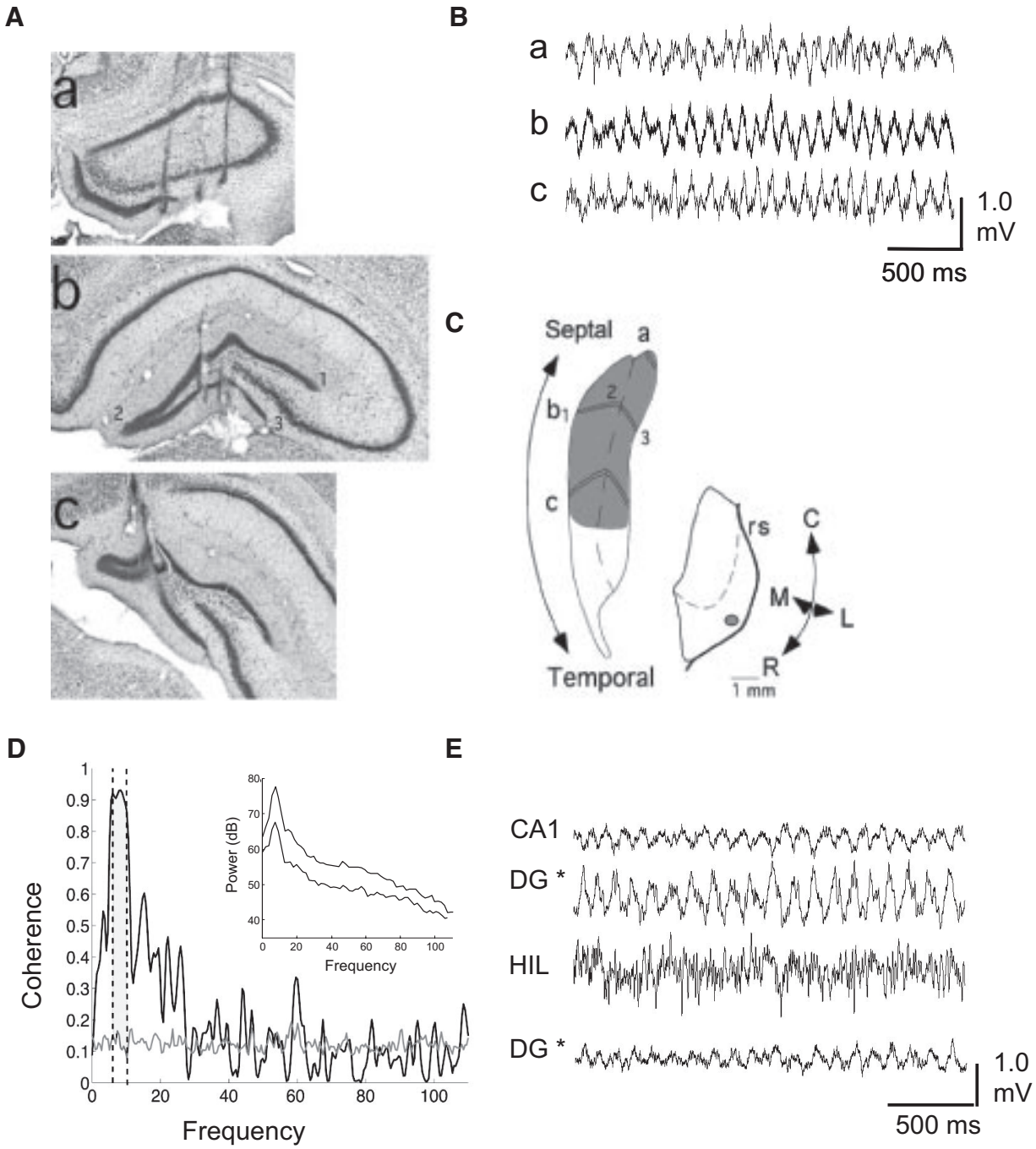

FIG. 1. Theta and gamma along the septotemporal axis of the hippocampus. *A*: photomicrograph showing tracts from electrode arrays positioned at 3 septotemporal (*a–c*) positions of the dentate gyrus (DG). Coronal sections correspond to positions (*a–c*) on flat map representation of the DG shown in *C*. Numerals 1–3 in photomicrograph correspond to the dorsal, apex, and ventral blade of DG shown in coronal strip (*b*) on the DG flat map. *B*: concurrent recordings from DG electrode sites shown in *A* illustrate subtle amplitude and phase shifts between DG electrodes that contribute to coherence differences along the septotemporal axis of the DG. *C*: flat map representations of the DG and entorhinal cortex (adapted from Swanson et al. 1978) illustrate the highly divergent innervation of the septal 50% of the DG (grayed area on DG flat map) from an anterograde tracer (gray dot) injection (bDA) within the lateral band of the entorhinal cortex. Injections at any site adjacent the rhinal sulcus (rs) in the rostral or caudal direction from the injection site illustrated innervate the same grayed area within the DG (Dolofo and Amaral 1998b). The position of each electrode was plotted on flatmap of the DG or CA1 (not shown), and the approximate distance between electrodes was measured in millimeters along the septotemporal axis. *D*: coherence as a function of frequency (black line). A normalized coherence value was calculated as the area above the 95% confidence interval of shuffled signals (gray line) for each electrode pair exhibiting theta peaks between 6 and 10 Hz. *Inset*: power spectra for DG signals shown (DG *) in *E*. Note high coherence despite amplitude difference of signals. *E*: laminar profile of theta and gamma oscillations. Note the prominent theta oscillations and phase reversal of signal present in the CA1 and DG traces as well as the prominent gamma oscillations in the hilus (HIL).

2, *B* and *C*, the decrease in theta is linear over the 5-mm distance examined in both the DG and hilar regions (DG: $y = -0.099x + 0.905$, $R^2 = 0.423$; HIL: $y = -0.063x + 0.633$, $R^2 = 0.223$), whereas the decrease in gamma is exponential in the same electrodes (DG: $y = 0.669e\text{-}0.57x$, $R^2 = 0.689$; HIL: $y = 0.636e\text{-}0.38x$, $R^2 = 0.732$). Coherence across 20-Hz

Downloaded from jn.physiology.org on September 19, 2011

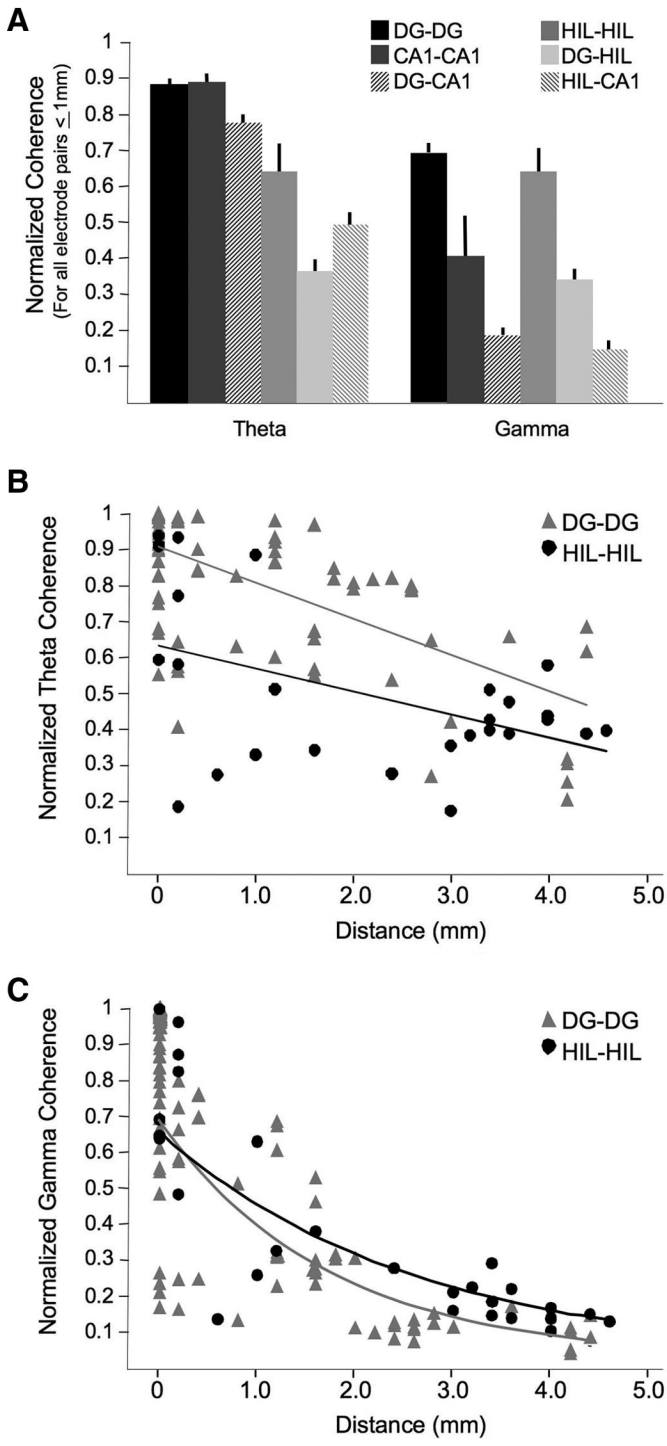

FIG. 2. Coherence varies across lamina and decreases as a function of septotemporal distance. *A*: Normalized theta and gamma coherences within and across lamina for all electrode pairs located within 1 mm. Both theta and gamma coherences vary as a function of lamina. Note that theta coherence is higher for DG electrodes than for HIL electrodes ($P < 0.01$) and that gamma coherence is higher in DG and HIL than in CA1 ($P < 0.01$). *B*: scatter plot showing normalized theta coherence between all DG-DG and HIL-HIL electrode pairs. Theta coherence decreases linearly with distance in both lamina (r^2 DG = 0.423; HIL = 0.223). *C*: scatter plot showing normalized gamma coherence within DG and hilar regions. Gamma coherence decreases exponentially for both DG and HIL regions (r^2 DG = 0.689; HIL = 0.732).

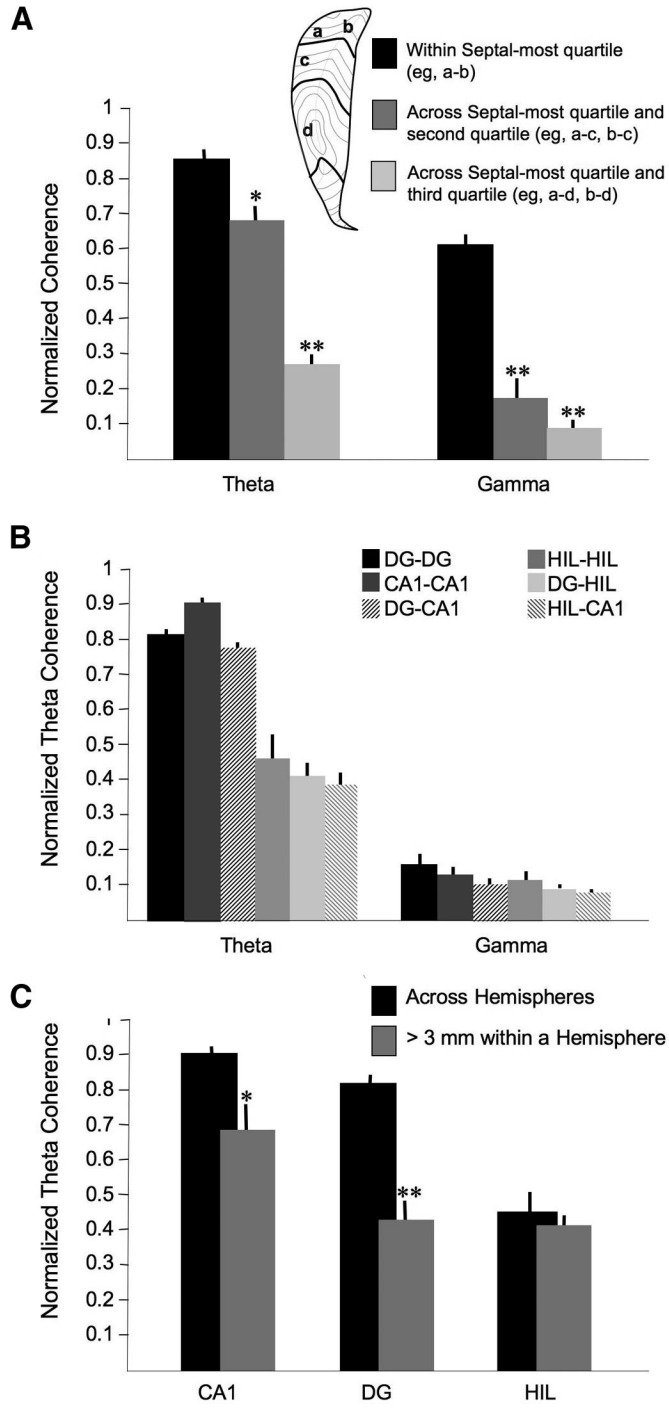

FIG. 3. Theta and gamma coherence decreases along the septotemporal axis of the hippocampus, while theta is more coherent across hemispheres. *A*: coherence between DG electrodes pairs was compared: between electrodes pairs within the septal-most quartile; electrode pairs spanning the 1st and 2nd quartile and electrode pairs spanning the 1st and 3rd quartile. Theta and gamma coherence was significantly higher for pairs in which both electrodes were located within the septal most quartile of the DG than for pairs spanning the 1st and 2nd or 1st and 3rd quartiles [$F(2,72) > 15.00$, * $P < 0.01$, ** $P < 0.001$]. *B*: theta is highly coherent at electrodes located in homotypic positions across hemispheres in the DG and CA1 regions but less so in the hilar regions. In contrast, gamma is only minimally coherent across hemispheres in all regions. *C*: theta coherence in DG and CA1 is significantly higher across hemispheres than at distances >3 mm within a hemisphere (*$P < 0.01$, ** $P < 0.001$). Theta coherence in the hilus is at a comparable level across hemisphere and at distances >3 mm.

Downloaded from jn.physiology.org on September 19, 2011

frequency bands from 30 to 110 Hz as well as across the beta band (16–30 Hz) is illustrated in Fig. 4. The decrease in coherence with distance was similar across all sub-bands. Our observations indicate a fairly steep decrease in gamma coherence (integrated between 40 and 110 Hz or within any 20-Hz range) with coherence decreasing to ~0.3 within 1–2 mm during REM sleep. Gamma coherence was highest when electrodes were separated by <0.5 mm and decreased as the distance between the electrode pair increased (Figs. 2, *A* and *C,* and 4).

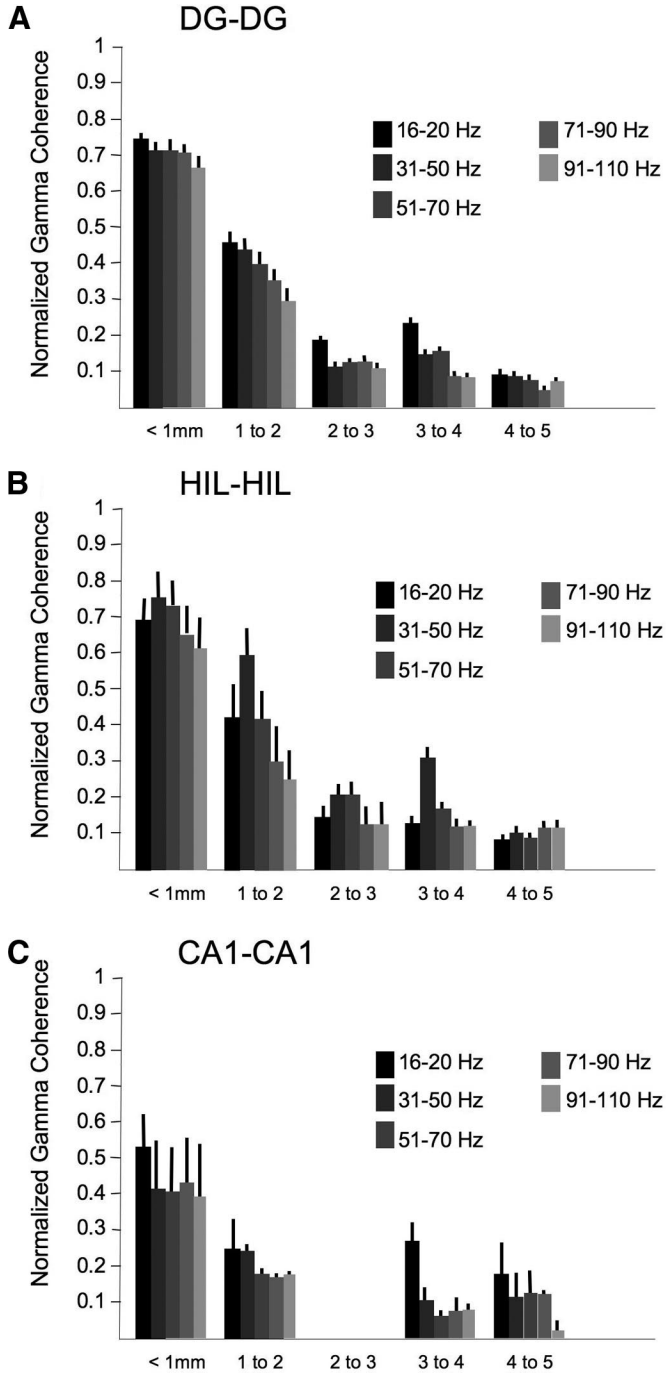

FIG. 4. Gamma decreases similarly with distance across all sub-bands. Gamma is typically defined in a broad band across ~40–110 Hz with the dominant frequency varying considerably. Gamma was divided into ~20-Hz frequency bands from 30 to 110 Hz to examine coherence in DG (*A*), HIL (*B*), and CA1 (*C*). The degree of decrease with distance was similar across all sub-bands.

Gamma coherence was notably higher between pairs of electrodes both in the dentate, or both in the hilus, than between CA1 pairs (see Figs. 2*A,* 3*B,* and 4) (see also Csiscvari et al. 2003). While gamma coherence within both the dentate and hilus was high, coherence between dentate and hilar sites was much lower, suggesting the presence of multiple gamma generators within the DG. In contrast to previous observations of high gamma coherence (~0.4–0.6) across hemispheres in mouse hippocampus (Buzsaki et al. 2003), there was little coherence across comparable laminar position in the contralateral hemisphere (Fig. 3*B*).

DISCUSSION

Foremost, we demonstrate that theta coherence decreases along the septotemporal (long) axis of the hippocampus. Second, theta is more coherent within homotypic regions (e.g., DG to DG, CA1 to CA1) across hemispheres than between physically closer homotypic sites within one hemisphere. Third, while theta is coherent for ≥5–6 mm, gamma coherence drops precipitously along the long axis as a function of distance. Fourth, we illustrate the low coherence of gamma recorded at dentate as compared with hilar sites. Last, unlike theta, gamma coherence is low (<0.4) across the laminar axis (DG to CA1) and is minimally coherent (<0.1) across hemispheres. These findings illustrate anatomic variation in theta and gamma signals across the long axis of the hippocampus during REM sleep. These data have implications for understanding the architecture determining extracellular current flow recorded as theta and gamma field potentials and suggest functional variability along the long axis.

Theta coherence varies with septotemporal distance within a hemisphere

Theta coherence decreased across the long axis of both the DG and CA1 [to values of 0.4 (DG-DG) and 0.7 (CA1-CA1) within 3 mm]. One might suspect that theta coherence would be higher along the long axis of the DG given the greater areal divergence of the entorhinal input to the dentate as compared with CA1. The entorhinal input to the DG actually dissects the folded sheet of dentate neurons into three broad domains along the long axis (see Fig. 1*C*). While theta coherence decreased along both the DG and CA1, coherence along CA1 was higher for each distance sampled (see Figs. 3*C* and 5). Thus while theta is a fairly global signal that is "coherent" throughout the hippocampus (see Bullock et al. 1990), there is considerable variation along the long axis.

Theta was more coherent (values of 0.8–0.9) between homotypic sites in the contralateral hemisphere of the septal hippocampus as compared with less distant sites within the same hemisphere (see Fig. 5). This finding highlights that coherence is not a function of distance but rather of anatomy (Bullock et al. 1990; Csiscvari et al. 2003) and the important role of the bilateral CA3/mossy cell projections (see Kocsis et al. 1984). The fact that theta coherence varies within the target zone of the lateral band entorhinal input suggests that the entorhinal input does not necessarily "dominate " theta current generation during REM sleep. Coherence along the long axis

Downloaded from jn.physiology.org on September 19, 2011

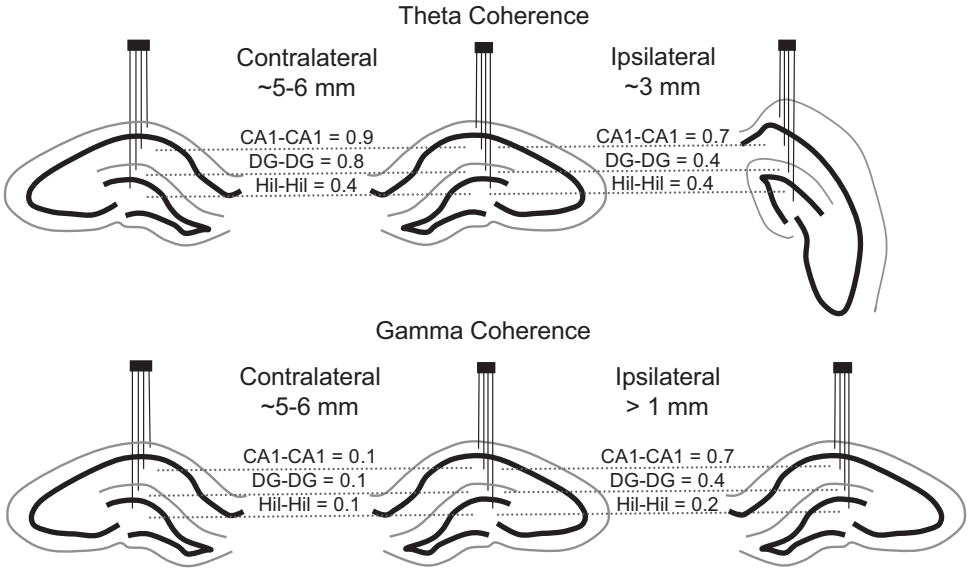

FIG. 5. Summary of theta and gamma coherence across long axis of the hippocampus. Figure summarizes theta (*top*) and gamma (*bottom*) coherence values between homotypic (e.g., CA1-CA1, DG-DG) positions across hemispheres (values shown in center) and at homotypic sites distant along the ipsilateral hemisphere.

varies more directly with the anatomy of the CA3/mossy cell projection. In contrast to the largely unilateral entorhinal input, both CA3 neurons and related mossy cells in the hilus project extensively along the long axis and across hemispheres in the rodent (Amaral and Witter 1995; Ishizuka et al. 1990; Li et al. 1994).

The extracellular currents generated in the dendritic field of granule and CA1 neurons is a dynamic product of excitation from mossy cell, CA3, and entorhinal inputs, and sculpting by somatic and dendritic inhibition (Ang et al. 2005; Kocsis et al. 1998). Using an in vitro preparation, Coulter and colleagues (Ang et al. 2005) demonstrated that maximal current flow within CA1 dendrites depends on specifically timed interactions between CA3 inputs and dendritic-targeting GABAergic neurons. Input from dendritic-targeting interneurons can maximize intracellular current flow to subsequent entorhinal input within very narrow (20 ms) time windows. Such currents are the origin of extracellular field potentials recorded during in vivo theta. One may imagine how the window of optimization in vivo depends on both theta frequency and the relative timing and strength of CA3 and entorhinal inputs. Such dynamics likely shape current flow in the dendritic field of the granule cells, where inputs from the lateral and medial entorhinal cortex are influenced by inputs from the mossy cells (Buckmaster et al. 1992, 1996). At various laminar positions along the dendrites of CA1 and granule neurons, entorhinal and CA3/mossy cell inputs interact to create the extracellular currents known as theta. Variability in the contribution of these excitatory inputs determines which subsets of granule, CA3, and CA1 cells discharge on a given theta cycle.

Gamma: focal synchrony

The current findings illustrate the focal distribution of gamma field potentials at distinct hippocampal sites. Gamma coherence decreased within 1–2 mm and diminished to minimal values within 2–3 mm. Gamma coherence, like theta, was higher between lamina-specific electrode pairs across the long axis (DG to DG and CA1 to CA1) than across lamina at similar longitudinal positions (DG to CA1). Glovelli and colleagues (2005) have emphasized the degree of gamma coherence across the transverse axis of CA3 in vitro and highlighted the focal distribution of gamma synchrony as compared with theta. We note limited coherence (<0.3) between gamma recorded at dentate compared with nearby hilar sites. This suggests independent gamma generators within the dentate. It would be useful to determine the degree of coherence between these hilar sites and nearby CA3 sites (see Csiscvari et al. 2003). On this note, Montgomery and colleagues have reported focal increases in theta and gamma synchrony across laminar sites in the DG, CA3, and CA1 of the septal hippocampus during phasic REM as compared with tonic REM. Phasic REM represents a unique REM state that occurs infrequently ($<5\%$ of total REM), and it would be of interest to determine the factors that contribute to generation of this unique REM state.

Theta, gamma, local circuits, the areal axis and functional differentiation

Theta and gamma provide a mechanism for bringing subsets of interconnected neurons together in time to form transient ensembles. Theta and gamma dynamics depend on the intrinsic properties of neuronal subtypes, local network interactions, and large-scale interactions across networks. Several circuit elements contribute to synchrony among hippocampal neurons. First, networks of distinct GABAergic neurons (e.g., basket cells, subclasses of dendritic-targeting cells) interact among themselves to create theta and gamma rhythms (e.g., Banks et al. 2000; Rotstein et al. 2005). These local GABA networks receive a select GABAergic input from the medial septum that may coordinate synchrony among regional and areal networks of GABA neurons (Buzsaki and Chrobak 1995; Freund and Antal 1988). GABAergic hippocamposeptal neurons also provide feedback to medial septal GABAergic, cholinergic and glutamatergic neurons that contribute to theta and gamma rhythmicity (e.g., Manseau et al. 2008).

Playing on hippocampal GABAergic networks and the pyramidal and granule neurons they regulate are the CA3/hilar and entorhinal inputs that provide rhythmic excitation at both theta and gamma frequency. These excitatory inputs include the entorhinal input to all hippocampal subfields as well as the CA3 and mossy cell input to CA1 and the DG, respectively.

Downloaded from jn.physiology.org on September 19, 2011

These inputs synapse in lamina- and area (longitudinal)-specific fashion on the dendritic field of granule, CA3, and CA1 neurons, contributing to the laminar (e.g., DG vs. CA1) and, as presently demonstrated, longitudinal variability in theta coherence. Thus a number of excitatory inputs, local and extrinsic inhibitory circuits as well as subcortical modulatory inputs provide multiple sources of dynamic range for theta and gamma synchronization.

Our laboratory is interested in synchronicity in theta along the septotemporal axis and its relation to the organization of entorhinal inputs. Anatomic and behavioral evidence would support functional differentiation of hippocampal circuits along the long axis (Bannerman et al. 2004; Strange et al. 1999). The long axis of the hippocampus is analogous to an areal region of the neocortex and receives input from circumscribed regions of the entorhinal cortex that in turn receive inputs from limited areas of associative cortex (Burwell and Amaral 1998; Chrobak and Amaral 2007; Dolorfo and Amaral 1998a,b; Lavenex et al. 2004). Entorhinal afferents may create sectors of functional network interactions along the longitudinal axis of the hippocampus. Despite the large number of studies examining theta in the rat and changes in theta power (e.g., Whishaw and Vanderwolf 1973; Wyble et al. 2004), few have examined theta or gamma coherence as a function of state or context (see, however, Kay 2005). Human studies have shown increased theta or gamma coherence in relation to state, cognitive processing and subsequent memory performance (Fell et al. 2003; Klimesch et al. 2006). Raghavachari et al. (2005) demonstrate that theta generated during the performance of a working memory task in multiple neocortical sites is not particularly coherent across distal neocortical electrodes but rather varied as a function of distance. Importantly, differences in connectivity, while often correlated with physical distance, are more likely key to differences in coherence. Thus we observed high coherence between electrode pairs in homotypic positions across hemispheres that were much more coherent than physically distant sites within a hippocampal hemisphere. The well-described topographic anatomy of the rodent hippocampus make it particularly suited for assessing the degree of synchrony across this structure and determining the conditions that contribute to its dynamic range. Further studies examining coherence along the long axis during different theta states (e.g., exploratory activity, attentive awake, novelty), or in relation to cognitive performance, may contribute to our understanding of functional variability along the longitudinal axis of the hippocampus.

ACKNOWLEDGMENTS

We thank Dr. Bernat Kocsis, Dr. Nancy Kopell, and C. Rossi for discussion and suggestions on this manuscript.

GRANTS

Funding for this work was provided by National Science Foundation Grant 0090451.

REFERENCES

Amaral DG, Witter MP. The three-dimensional organization of the hippocampal formation: a review of anatomical data. *Neuroscience* 31: 371–391, 1995.

Ang CW, Carlson GC, Coulter DA. Hippocampal CA1 circuitry dynamically gates direct cortical inputs preferentially at theta frequencies. *J Neurosci* 25: 9567–9580, 2005.

Banks MI, White JA, Pearce RA. Interactions between distinct GABA(A) circuits in hippocampus. *Neuron* 25: 449–457, 2000.

Bannerman DM, Rawlins JN, McHugh SB, Deacon RM, Yee BK, Bast T, Zhang WN, Pothuizen HH, Feldon J. Regional dissociations within the hippocampus–memory and anxiety. *Neurosci Biobehav Rev* 28: 273–283, 2004.

Bland BH. Physiology and pharmacology of hippocampal formation theta rhythms. *Prog Neurobiol* 26: 1–54, 1986.

Bragin A, Jando G, Nadasdy Z, Hetke J, Wise K, Buzsaki G. Gamma (40–100 Hz) oscillation in the hippocampus of the behaving rat. *J Neurosci* 15: 47–60, 1995.

Brankack AJ, Stewart M, Fox SE. Current source density analysis of the hippocampal theta rhythm: associated sustained potentials and candidate synaptic generators. *Brain Res* 615: 310–327, 1993.

Buckmaster PS, Strowbridge BW, Kunkel DD, Schmiege DL, Schwartzkroin PA. Mossy cell axonal projections to the dentate gyrus molecular layer in the rat hippocampal slice. *Hippocampus* 2: 349–362, 1992.

Buckmaster PS, Wenzel HJ, Kunkel DD, Schwartzkroin PA. Axon arbors and synaptic connections of hippocampal mossy cells in the rat in vivo. *J Comp Neurol* 366: 271–292, 1996.

Bullock TH, Buzsaki G, McClune MC. Coherence of compound field potentials reveals discontinuities in the CA1-subiculum of the hippocampus of the freely-moving rat. *Neuroscience* 38: 609–619, 1990.

Burwell RD, Amaral DG. Perirhinal and postrhinal cortices of the rat: interconnectivity and connections with the entorhinal cortex. *J Comp Neurol* 391: 293–321, 1998.

Buzsaki G. Theta oscillations in the hippocampus. *Neuron* 33: 325–340, 2002.

Buzsaki G, Buhl DL, Harris KD, Csicsvari J, Czeh B, Morozov A. Hippocampal network patterns of activity in the mouse. *Neuroscience* 16: 201–211, 2003.

Buzsaki G, Chrobak JJ. Temporal structure in spatially organized neuronal ensembles: a role for interneuronal networks. *Curr Opin Neurobiol* 5: 504–510, 1995.

Buzsaki G, Czopf J, Kondakor I, Kellenyi L. Laminar distribution of hippocampal rhythmic slow activity (RSA) in the behaving rat: current source density analysis, effects of urethane and atropine. *Brain Res* 365: 125–137, 1986.

Buzsaki G, Leung L, Vanderwolf CH. Cellular basis of hippocampal EEG in the behaving rat. *Brain Res Rev* 6: 139–171, 1983.

Chrobak JJ, Amaral DG. The entorhinal cortex of the monkey. VII. Intrinsic connections. *J Comp Neurol* 500: 612–633, 2007.

Chrobak JJ, Buzsaki G. Gamma oscillations in the entorhinal cortex of the freely behaving rat. *J Neurosci* 18: 388–398, 1998.

Csicsvari J, Jamieson B, Wise KD, Buzsaki G. Mechanisms of gamma oscillations of the behaving rat. *Neuron* 37: 311–322, 2003.

Cunningham MO, Davies CH, Buhl EH, Kopell N, Whittington MA. Gamma oscillations induced by kainate receptor activation in the entorhinal cortex in vitro. *J Neurosci* 23: 9761–9769, 2003.

Dickson CT, Biella G, de Curtis M. Evidence for spatial modules mediated by temporal synchronization of carbachol-induced gamma rhythm in medial entorhinal cortex. *J Neurosci* 20: 7846–7854, 2000.

Dolorfo CL, Amaral DG. Entorhinal cortex of the rat: organization of intrinsic connections. *J Comp Neurol* 398: 49–82, 1998a.

Dolorfo C, Amaral DG. Entorhinal cortex of the rat: topographic organization of the cells of origin of the perforant path projections to the dentate gyrus. *J Comp Neurol* 398: 25–48, 1998b.

Efron B, Tibshirani, RJ. *An Introduction to the Bootstrap.* New York: Chapman and Hall. 1993.

Fell J, Klaver P, Elfadil H, Schaller C, Elger CE, Fernandez G. Rhinal-hippocampal theta coherence during declarative memory formation: interaction with gamma synchronization? *Eur J Neurosci* 17: 1082–1088, 2003.

Freund TF, Antal M. GABA-containing neurons in the septum control inhibitory interneurons in the hippocampus. *Nature* 336: 170–173, 1988.

Gray CM. Synchronous oscillations in neuronal systems: mechanisms and functions. *Cog Neurosci* 1: 11–38, 1994.

Gloveli T, Dugladze T, Rotstein HG, Traub RD, Monyer H, Heinemann U, Whittington MA, Kopell NJ. Orthogonal arrangement of rhythm-generating microcircuits in the hippocampus. *Proc Natl Acad Sci USA* 102: 13295–13300, 2005.

Hasselmo ME. What is the function of hippocampal theta rhythm? Linking behavioral data to phasic properties of field potential and unit recording data. *Hippocampus* 15: 936–949, 2005.

Downloaded from jn.physiology.org on September 19, 2011

Hasselmo ME, Bodelon C, Wyble BP. A proposed function for hippocampal theta rhythm: separate phases of encoding and retrieval enhance reversal of prior learning. *Neural Comput* 14: 793–817, 2002.

Hyman JM, Zilli EA, Paley AM, Hasselmo ME. Medial prefrontal cortex cells show dynamic modulation with the hippocampal theta rhythm dependent on behavior. *Hippocampus* 15: 739–749, 2005.

Ishizuka N, Weber J, Amaral DG. Organization of intrahippocampal projections from CA3 pyramidal cells in the rat. *J Comp Neurol* 295: 580–623, 1990.

Jones MW, Wilson MA. Theta rhytms coordinate hippocampal-prefrontal interactions in a spatial memory task. *PLOS Biol* 3: e402, 2005.

Kahana MJ, Seelig D, Madsen JR. Theta returns. *Curr Opin Neurobiol* 11: 739–744, 2001.

Kay LM. Theta oscillations and sensorimotor performance. *Proc Natl Acad Sci USA USA* 102: 3863–3868, 2005.

Klimesch W, Hanslmayr S, Sauseng P, Gruber W, Brozinsky CJ, Kroll NE, Yonelinas AP, Doppelmayr M. Oscillatory EEG correlates of episodic trace decay. *Cereb Cortex* 16: 280–290, 2006.

Kocsis B, Bragiin A, Buzsaki G. Interdependence of multiple theta generators in the hippocampus: a partial coherence analysis. *J Neurosci* 19: 6200–6212, 1999.

Kocsis B, Thinschmidt JS, Kinney GG, Vertes RP. Seperation of hippocampal theta dipoles by partial coherence analysis in the rat. *Brain Res* 660: 341–345, 1994.

Lavenex P, Suzuki WA, Amaral DG. Perirhinal and parahippocampal cortices of the macaque monkey: intrinsic projections and interconnections. *J Comp Neurol* 472: 371–394, 2004.

Leung L-WS. Model of gradual phase shift of theta rhythm in rat. *Electroencephalogr Clin Neurophysiol* 52: 1051–1065, 1984.

Lisman J. The theta/gamma discrete phase code occurring during the hippocampal phase precession may be a more general brain coding scheme. *Hippocampus* 15: 913–922, 2005.

Li XG, Somogyi P, Ylinen A, Buzsaki G. The hippocampal CA3 network: an in vivo intracellular labeling study. *J Comp Neurol* 339: 181–208, 1994.

Lin B, Kramar EA, Bi X, Brucher FA, Gall CM, Lynch G. Theta stimulation polymerizes actin in dendritic spines of hippocampus. *J Neurosci* 25: 2062–2069, 2005.

Manseau F, Goutagny R, Danik M, Williams S. The hippocamposeptal pathway generates rhythmic firing of GABAergic neurons in the medial septum and diagonal bands: an investigation using a complete septohippocampal preparation in vitro. *J Neurosci* 28: 4096–4107, 2005.

Maurer AP, VanRhoads SR, Sutherland GR, Lipa P, McNaughton BL. Self-motion and the origin of differential spatial scaling along the septo-temporal axis of the hippocampus. *Hippocampus* 15: 841–852, 2005.

Montgomery SM, Sirota A, Buzsaki G. Theta and gamma coordination of hippocampal networks during waking and rapid eye movement sleep. *J Neurosci* 28: 6731–6741, 2008.

Petsche H, Stumpf C, Gogolak G. The significance of the rabbit's septum as a relay station between the midbrain and the hippocampus. I. The control of hippocampus arousal activity by the septum cells. *Electroencephalogr Clin Neurophysiol* 14: 2020–2011, 1962.

Raghavachari S, Lisman JE, Tully M, Madsen JR, Bromfield EB, Kahana MJ. Theta oscillations in human cortex during a working-memory task: evidence for local generators. *J Neurophysiol* 95: 1630–1638, 2006.

Roark RM, Escabi MA. B-spline design of maximally flat and prolate spheroidal-type FIR filters. *IEEE Trans Signal Process* 47: 701–716, 1999.

Rotstein HG, Pervouchine DD, Acker CD, Gillies MJ, White JA, Buhl EH, Whittington MA, Kopell N. Slow and fast inhibition and an H-current interact to create a theta rhythm in a model of CA1 interneuron network. *J Neurophysiol* 94: 1509–1518, 2005.

Strange BA, Fletcher PC, Henson RN, Friston KJ, Dolan RJ. Segregating the functions of human hippocampus. *Proc Natl Acad Sci USA* 96: 4034–4039, 1999.

Swanson LW, Wyss JM, Cowan WM. An autoradiographic study of the organization of intrahippocampal association pathways in the rat. *J Comp Neurol* 181: 681–715, 1978.

Vertes RP, Kocsis B. Brainstem-diencephalo-septohippocampal systems controlling the theta rhythm of the hippocampus. *Neuroscience* 81: 893–926, 1997.

Vinogradova OS. Expression, control, and probable functional significance of the neuronal theta-rhythm. *Prog Neurobiol* 45: 523–583, 1995.

Welch PD. The use of fast Fourier transform fot he estimation of power spectra: a method based on time averaging over short, modified periodograms. *IEEE Trans Audio Electroacoust* 15: 70–73, 1967.

Whishaw IQ, Vanderwolf CH. Hippocampal EEG and behavior: changes in amplitude and frequency of RSA (theta rhythm) associated with spontaneous and learned movement patterns in rats and cats. *Behav Biol* 8: 461–484, 1973.

Wyble BP, Hyman JM, Rossi CA, Hasselmo ME. Analysis of theta power in hippocampal EEG during bar pressing and running behavior in rats during distinct behavioral contexts. *Hippocampus* 14: 662–674, 2004.

Downloaded from jn.physiology.org on September 19, 2011